ACS APPLIED MATERIALS & INTERFACES

Research Article

www.acsami.org

Rapid Large-Scale Assembly and Pattern Transfer of One-Dimensional Gold Nanorod Superstructures

Rana Ashkar,[*,†,‡,§,◆] Michael J. A. Hore,[*,∥,◆] Xingchen Ye,[⊥,¶] Bharath Natarajan,[#] Nicholas J. Greybush,[○] Thomas Lam,[#] Cherie R. Kagan,[⊥,∇,○] and Christopher B. Murray[⊥,○]

[†]Center for Neutron Research, National Institute of Standards and Technology (NIST), Gaithersburg, Maryland 20899, United States

[‡]Materials Science and Engineering Department, University of Maryland, College Park, Maryland 20742, United States

[§]Biology and Soft Matter Division, Neutron Sciences Directorate, Oak Ridge National Laboratory, Oak Ridge, Tennessee 37831, United States

[∥]Department of Macromolecular Science & Engineering, Case Western Reserve University, 10900 Euclid Avenue, Cleveland, Ohio 44106, United States

[⊥]Department of Chemistry, University of Pennsylvania, 231 South 34th Street, Philadelphia, Pennsylvania 19104, United States

[#]Center for Nanoscale Science and Technology, National Institute of Standards and Technology (NIST), Gaithersburg, Maryland 20899, United States

[∇]Department of Electrical and Systems Engineering, University of Pennsylvania, 200 South 33rd Street, Philadelphia, Pennsylvania 19104, United States

[○]Department of Materials Science & Engineering, University of Pennsylvania, 3231 Walnut Street, Philadelphia, Pennsylvania 19104, United States

Supporting Information

ABSTRACT: The utility of gold nanorods for plasmonic applications largely depends on the relative orientation and proximity of the nanorods. Though side-by-side or chainlike nanorod morphologies have been previously demonstrated, a simple reliable method to obtain high-yield oriented gold nanorod assemblies remains a significant challenge. We present a facile, scalable approach which exploits meniscus drag, evaporative self-assembly, and van der Waals interactions to precisely position and orient gold nanorods over macroscopic areas of 1D nanostructured substrates. By adjusting the ratio of the nanorod diameter to the width of the nanochannels, we demonstrate the formation of two highly desired translationally ordered nanorod patterns. We further demonstrate a method to transfer the aligned nanorods into a polymer matrix which exhibits anisotropic optical properties, allowing for rapid fabrication and deployment of flexible optical and electronic materials in future nanoscale devices.

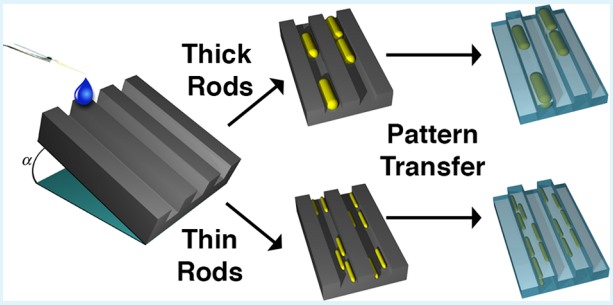

KEYWORDS: *gold nanorods, end-to-end assembly, controlled positional order, plasmonics, polymer nanocomposites*

INTRODUCTION

Gold nanorods (Au NRs) possess highly tunable optical absorption due to the dependence of their surface plasmon resonances (SPRs) on aspect ratio. Because of two distinct length scales along the transverse and longitudinal directions of the nanorod, two surface plasmon resonances exist at wavelengths that depend on the diameter and aspect ratio of the nanorod, respectively,[1] which allows tuning the SPR by varying these two dimensions. In fact, unlike spherical gold nanoparticles, gold nanorods can be tuned to absorb light over a wide wavelength range from around 600 nm to well into the near-infrared spectrum (>1100 nm). This tunability and broad range of optical absorption renders Au NRs as attractive candidates for use in optical devices, surface-enhanced Raman spectroscopy (SERS) substrates, and biological or molecular recognition techniques.[2] In addition to the size-dependent extinction, the plasmonic response of gold nanorods is highly sensitive to the proximity and orientation of neighboring nanorods, which has driven significant research efforts on the design of nanorod assemblies for advanced technological applications. In many such applications, there is a growing need for precise positioning[3] and directionality[4] of gold nanorods on substrates or in matrices if they are to enjoy widespread use in nanoscale devices.

To date, obtaining highly ordered gold nanorods within a material remains an outstanding challenge. Two types of

Received: May 5, 2017
Accepted: July 7, 2017
Published: July 7, 2017

DOI: 10.1021/acsami.7b06273
ACS Appl. Mater. Interfaces 2017, 9, 25513−25521

assembly are primarily considered for plasmonic applications: side-by-side and end-to-end arrangements, which, respectively, exhibit increasing blue and red shifting of the SPR with decreasing rod−rod separation.[5] While several methods, mainly based on depletion−attraction forces, have been demonstrated for side-by-side alignment of nanorods in solution[6,7] and in polymer melts,[8,9] a quick and reliable method for precise positioning of close-proximity nanorods in parallel or end-to-end assemblies remains a challenge.[10] The largest hurdle in obtaining these structures is devising methods to overcome the strong rod−rod interactions that favor compact side-by-side NR assembly. The case of end-to-end assembly is particularly challenging as it requires site-specific linking of nanorods, but a few techniques have been successfully developed for end-linking Au NRs, including driving the assembly by end-functionalizing Au NRs and subsequently tuning solvent quality,[11−13] using molecular bridging,[14,15] or taking advantage of the preferential bonding of capping molecules.[16,17] Ferrier and co-workers[16] demonstrated that, once linked in solution, nanorod chains could be transferred into a polymer matrix; however, the chains did not have a significant persistence length, which reduces both the ability of the nanocomposite to harvest polarized light and the anisotropy of the optical properties of the nanocomposite. Chain assemblies of nanorods were also recently demonstrated on lithographically structured polymers[18] and patterned block copolymer films,[19] but these assemblies lacked well-defined orientational order of the nanorods within the chains, which can be detrimental for material designs requiring strong plasmonic field coupling. Nepal and co-workers[20] were able to obtain long-range translational order of Au NRs cast from solution onto oriented poly(styrene)-*b*-poly(2-vinylpyridine) (PS-*b*-P2VP) films by exploiting preferential interactions between the nanorods and the P2VP block. However, the resulting chainlike assemblies were characterized by a noncompact nanorod assembly and had larger-than-desired distances between adjacent nanorods. Ahmed et al.[21] adopted a similar approach to direct the self-assembly of Au NRs to hydrophilic stripes, while Liz-Marzán's group[22] used a poly(dimethylsiloxane) (PDMS) template to confine Au NRs and induce vertical, side-by-side alignment as drying occurred. Composto's group used the lamellar phase of a PS-*b*-poly(methyl methacrylate) (PMMA) diblock copolymer to confine and orient Au NRs in the transverse direction of a polymer film, but the in-plane orientation was still isotropic.[23] To date, this method has not yet been successfully applied to other block copolymer morphologies. Other methods, such as mechanical stretching of polymer films[24] and electrospinning of fibers,[25] have successfully oriented Au NRs, but these methods were not able to obtain a high degree of nanorod order across macroscopic length scales. One of the most promising methods to date involves exploiting capillary forces to place and align Au NRs on a templating substrate.[18,22,26−29] A notable example of such an approach is the recent work by Fery et al.[27] in which the plasma etching of PDMS was used to create wrinkled PDMS substrates with a thin surface layer of SiO_2, and a dip coating method was used for nanorod patterning along the direction of the wrinkles. They showed that the nanorods formed multilayered structures, side-by-side-oriented Au NRs, or single-file aligned Au NRs depending on the amplitude of the wrinkle. The aligned Au NRs could then be transferred onto indium tin oxide (ITO) substrates using wet-contact printing. The authors noted, however, that as-synthesized Au NRs could not be aligned, requiring Au NRs that were functionalized with proteins such as bovine serum albumin (BSA). While this approach successfully produced optical metamaterials with highly aligned Au NRs, key drawbacks include the requirement to functionalize Au NRs with proteins, the presence of dislocations in the wrinkled PDMS, the sole reliance on wrinkle geometry to control ordered structures, and side-by-side clustering of the nanorods in wrinkles wider than the nanorod diameter. Flauraud et al. recently took a similar approach, and created lithographically defined templates with which they could assemble Au NRs into predefined patterns.[30] Motivated by previous work, and taking advantage of recent advances in Au NR synthesis, we hypothesized that, by manipulating geometry and taking advantage of strong Au−Si interactions, it would be possible to align and position Au NRs over macroscopic length scales, tune the characteristics of the assembled nanorod structures, and transfer the particles into a polymeric material that would possess anisotropic optical properties.

In this work, we investigate the long-range alignment of Au NRs on nanostructured silicon gratings, and present a method which exploits meniscus drag, evaporative self-assembly, and short-range van der Waals forces to obtain highly oriented Au NRs over large length scales. We demonstrate that, by changing the ratio of the nanorod diameter (D_{NR}) to the groove width (w) of the grating, two distinct nanorod assemblies can be obtained. For Au NRs with diameters that are much smaller than w, we observe segregation of the nanorods to the walls of the grooves, and end-to-end alignment of Au NRs along the groove direction, which can be tuned to form two distinct files of nanorods in each unit cell. For Au NRs with diameters commensurate with w, nanorods form discrete, single-file chains along the groove direction, with persistence lengths that can be micron-scale. Finally, we demonstrate that the aligned nanorods can be readily transferred into a polymeric material within minutes to form a polymer nanocomposite with polarization-dependent light extinction, presenting many exciting opportunities for rapid device fabrication in the future.

EXPERIMENTAL METHODS

Materials. Gold nanorods were synthesized using a seed-mediated growth method following the procedures by Ye et al.[31,32] In this work, we used two nanorod batches with sizes (20 × 73) nm and (58 × 110) nm, which we refer to as thin and thick nanorods, respectively. The nanostructured silicon substrates were purchased from LightSmyth Technologies and were used as received without any surface treatment or coating. However, silicon is known to naturally form an oxide layer, the thickness of which was obtained by neutron reflectometry to be ∼2 nm. Reflectometry measurements (not shown here) were performed on beamline 4B at the Spallation Neutron Source at Oak Ridge National Laboratory. The substrates used in this work are periodic linear nanostamps (gratings) with a rectangular profile, a period of 140 nm, a channel depth of 50 nm, and a channel width of 70 nm. A cross-sectional SEM micrograph of the substrates is shown in Figure S1 in the Supporting Information. It is important to point out that gratings with different channel widths can be obtained, commercially or by e-beam lithography, for use with rods of different dimensions. This offers the possibility of tuning both channel width and rod dimensions for the generation of different nanorod assemblies. In the current work, the use of two nanorod sizes with a single channel width was sufficient for the comparative studies intended here. The grating identified above was chosen on the basis of the smallest channel width that is commercially available and that would provide the maximum possible confinement for the alignment of the nanorods described hereafter.

Small-Angle Neutron Scattering (SANS). SANS measurements were performed on aqueous suspensions of the CTAB-coated

DOI: 10.1021/acsami.7b06273
ACS Appl. Mater. Interfaces 2017, 9, 25513−25521

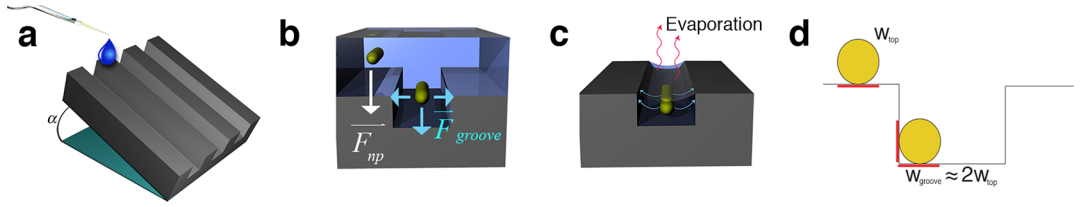

Figure 1. (a) Solution casting geometry showing the grating tilt (α) relative to a horizontal surface such that the grating lines are along the anticipated flow direction of the cast droplets. Parts b–d show schematic depictions of the forces acting on the nanorods. (b) Comparison of the short-range attraction forces on a nanorod on top of the mesa, F_{np}, vs those of a nanorod in the groove, F_{groove}, showing the energetic preference for nanorods to locate within the groove. (c) Capillary (blue lines) and evaporation-mediated (red lines) forces contributing to the nanorod assembly in the grooves. (d) Van der Waals interactions (W) on a thin nanorod interacting with a single surface near the top of the grooves vs those interacting with two surfaces near the corners of the grooves.

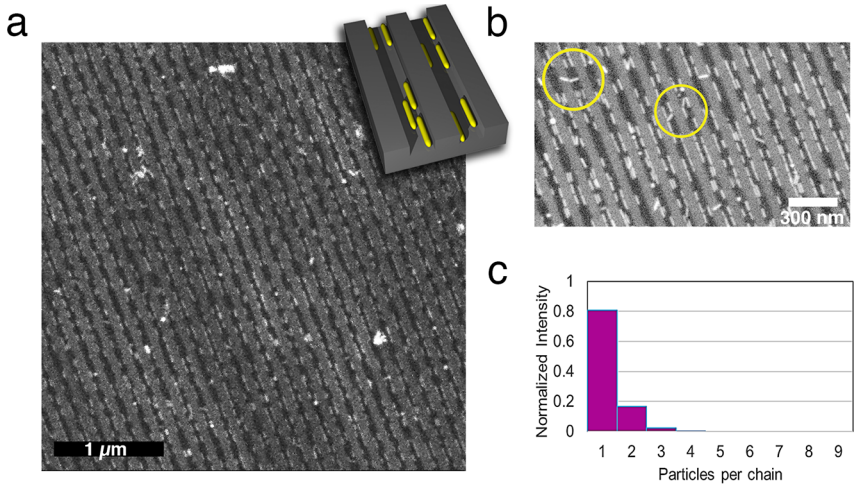

Figure 2. Oriented Au NRs with average diameter D_{NR} = 20.5 nm confined to grooves with width w = 70 nm. (a) Large-area scanning electron micrographs showing that Au NRs preferentially segregate to the walls of the silicon grooves, and are aligned along the direction of the groove. The schematic illustrates the alignment and location of Au NRs in the groove. (b) Higher-magnification image of the same sample, showing highly oriented, end-to-end-aligned, Au NR structures that persist over long length scales. (c) Image analysis of multiple micrographs showing an average of 1.20 ± 0.6 rods/chain and 4–6 rods in the longest observed chains.

(cetyltrimethylammonium bromide-coated) nanorods used in the solution casting method described in the main text. The experiments were conducted on the NG3 30m SANS beamline at the NIST Center for Neutron Research (NCNR). The suspensions were loaded in 2 mm demountable titanium cells available at the NCNR. The suspensions were sonicated for 30 min just before loading and the start of SANS measurements to break down aggregates and ensure good dispersion of the nanorods in solution. The SANS measurements were done in standard configuration covering a Q range 0.002–0.6 $Å^{-1}$, where Q is the wave vector transfer. Data reduction was performed using the Igor NCNR data reduction protocols which account for background subtraction, detector sensitivity, and empty beam corrections to obtain the absolute intensity pattern shown in Figure S2. The SANS data indicate highly monodisperse nanorods, as evident from the well-defined oscillations in the scattering pattern. The scattering data were fit to a core–shell cylinder model to extract both the nanorod and surfactant bilayer dimensions.

Scanning Electron Microscopy (SEM). SEM measurements of the NR-decorated gratings were performed using a Zeiss Supra-55VP field emission SEM in variable pressure mode and an FEI Helios Nanolab 650. Conducting copper thongs were applied to the surface of the grating to minimize charging effects. For the PMMS elastomer, the front "nanostructured" face of the stamp was coated with a thin layer of carbon using a Gatan high-resolution ion beam coater (Model 681) prior to the SEM measurement to eliminate charging effects, which are even more pronounced in the elastomer compared to those in silicon. The coating was applied using an ~8 keV ion beam on a carbon target for 1 min at a rate of 0.15 Å/s, yielding a carbon coating ~1 nm thick. SEM measurements were then performed using an FEI Helios Nanolab 650.

Dark Field Scattering Spectroscopy. Transmission dark field scattering spectra were collected by a CRAIC 308 PV micro-spectrophotometer integrated on an Olympus BX51 microscope. White light from a 100 W tungsten halogen lamp was focused onto the sample using a substage dark field condenser lens, and dark field scattering from the sample was collected by a 50× IR objective (Olympus LCPlan N IR, NA 0.65). The incident light was linearly polarized by a broad-band visible–NIR polarizer (Melles Griot) on a rotatable mount. The polarizer was rotated in increments of 30° over a 180° range. At 50× magnification, the collection aperture of the microspectrophotometer corresponded to a sample region of 5.3 μm × 5.3 μm. Spectra were collected over the wavelength range 350–1000 nm. The measured scattering intensity spectra were normalized by the lamp spectrum as measured in transmission bright field mode.

Orientational Analysis. Two-dimensional orientational analysis was performed on the SEM micrographs using different grid sizes, r. At each r, multiple boxes of size r are used to obtain statistically representative values of the 2D order parameter, $S_{2D}(r)$, as shown in Figure S6a.[33] The 2D order parameter is defined as

$$S_{2D}(r) = \frac{1}{N_{rod}} \sum_{i=1}^{N_{rod}} \cos 2\theta_i$$

where N_{rod} is the number of nanorods within a grid size r in the micrograph, and θ_i is the angle between nanorod i and the average orientation of the ensemble of rods within the region of size r (Supporting Information, Section 5). The uncertainty is obtained from

DOI: 10.1021/acsami.7b06273
ACS Appl. Mater. Interfaces 2017, 9, 25513–25521

the variation in these values. The measured values and the corresponding uncertainties are shown in Figure S6b for thin and thick nanorod samples. The average order parameter was obtained from the analysis of multiple micrographs ($n > 3$) with different grid sizes.

RESULTS AND DISCUSSION

Au NRs were synthesized using a seed-mediated growth method that has been extensively investigated in the literature, resulting in cetyltrimethylammonium bromide-coated (CTAB-coated) nanorods. High yields of monodisperse Au NRs were produced by the incorporation of small amounts of aromatic additives[21] or a cosurfactant sodium oleate[22] into the nanorod growth solution, as previously described by Ye and co-workers.[31,32] Small-angle neutron scattering (SANS) measurements confirm that the seed-mediated synthesis yields highly monodisperse nanorods with a CTAB coating of 3.61 ± 0.05 nm thickness, in accord with previous measurements by Gómez-Graña et al.[34] and Hore et al.[35] It is noted that all reported errors correspond to ±1 standard deviation. The nanorod assemblies were generated by solution casting onto 1 × 1 cm^2 silicon gratings with a 140 nm period, 70 nm groove width (w), and 50 nm groove depth (d). The gratings were inclined at approximately 5° with respect to a horizontal surface, as shown in Figure 1a. Aqueous solutions of Au NRs (~20 μL) were pipetted onto the grating surface near its elevated edge, allowing capillary forces to wick the liquid along the grating lines. The gratings were then covered with a glass Petri dish and allowed to dry slowly in a fume hood over the course of 2 h. A combination of short-range (Figure 1b), capillary, and evaporation-mediated (Figure 1c) forces resulted in the self-assembly of Au NRs along the groove direction. While SEM imaging on the gratings (Figure 2) cannot definitively determine the vertical location of the nanorods within the channels, we hypothesized that they are located in the bottom corners of the channels because of increased van der Waals interactions in this configuration. As shown schematically in Figure 1d, there are two interacting surfaces near the corners of the channel as opposed to the single surface close to the top or in the middle of the channel. This provides a thermodynamic driving force for positioning the nanorods deep in the channels and along the channel walls. In fact, the positioning of nanorods was later confirmed by SEM on the PMMS imprints of the assembled structures, as described later in the paper and shown in Figure S3 of the Supporting Information.

The tilted substrate geometry is essential for the assembly approach adopted in this work, and results in a concentration gradient of Au NRs along the groove direction. Although capillary forces naturally drag the cast fluid along the grooves, the tilt geometry ensures unidirectional flow of the solution along the lines of the grating and reduces the amount of excess solution on the top surface of the substrate. The shallow tilt angle used here ensures a slow flow of the solution along the grooves and allows the nanorods to reassemble at the meniscus front as it sweeps across the grating. In studying the coffee-ring effect[36] in suspensions of elongated colloids, Yodh et al.[37] found that ellipsoidal and rodlike particles are drawn to the edge of the meniscus along the flow direction and thus tend to deposit perpendicular to the meniscus front as the solvent evaporates. By tuning the speed of the meniscus front and the translational and rotational diffusion of the nanorods in solution, it is possible to deposit nanorods in chainlike patterns as the meniscus recedes. The deposition and assembly of particles depend on the wetting properties of the solution onto the grating material, the evaporation rate, as well as the concentration and viscosity of the nanorod solution.

Because of the concentration gradient in the sample, measurements were performed over three different regions of the substrate: low-nanorod-concentration regions near the top of the substrate, intermediate-concentration regions in the middle, and high-concentration regions close to the bottom. Figure 2a shows scanning electron micrographs of the long-range order of the assembly of the thin nanorods (D_{NR} = 20.5 nm) at an intermediate concentration, clearly demonstrating that the nanorods are confined within the grooves with remarkable segregation to the sidewalls. The segregation of particles to the sidewalls, to form two parallel channels, is a phenomenon that has not been observed in other capillary-force-based techniques, and is likely the result of van der Waals interactions between the Au NRs and the silicon grooves. The Au NRs remain almost perfectly oriented along the grooves over many micrometers, although a small number of regions exist where tilted orientations of Au NRs are observed, as indicated by yellow circles in Figure 2b which shows a selected higher-magnification micrograph of the sample in the same region. Image analysis of the corresponding micrographs (Figure 2c) shows that, on average, the Au NRs formed aligned chains with a maximum of 4−6 rods per chain (average of 1.2 ± 0.6 rods/chain). Regions with lower and higher nanorod concentrations are shown in Figures S3 and S7, respectively, in the Supporting Information. More detailed image analysis (Supporting Information, Figure S8) shows that as the filling fraction of Au NRs increases from approximately 9% to 29%, the percentage of Au NRs in two-file orientations decreases from 66% to 15%, while the percentage of side-by-side orientations increases from 29% to 85%. The observed two-file Au NR assembly opens up new possibilities not only for assembling nanorods in a chainlike structure but also for controlling the spacing between nanorod chains. Such a control over nanorod spacing was shown in a recent theoretical finite difference time domain (FDTD) calculation[38] to be of great potential in amplifying plasmon coupling and enhancing near-infrared tunability. While such patterns have been observed on spherical nanoparticles with chemically modified surfaces,[39] the gratings used in this work were not modified in any form. Going forward, chemical modification of the silicon surface using silane chemistry, for example, may present opportunities for further tuning of the nanorod assembly within the channels.

Several factors concomitantly contribute to the formation of the assembled structures depicted in Figure 2. Capillary forces and van der Waals interactions between the gold nanorods and the silicon substrate are expected to draw the nanorods into the channels. As shown schematically in Figure 1b,c, nanorods in the channels experience stronger net attractive forces compared to nanorods close to the grating mesas, which preferentially drives more nanorods into the channels. These forces favor NR alignment along the walls of the channels, thus lowering their energy state by maximizing their contact area. Simultaneous fluid-phase NR rearrangements near the grating surface contribute to the rod alignment in accord with Onsager's theory,[40] which describes spontaneous ordering of rigid colloidal rods by a simultaneous minimization of excluded volume and maximization of entropy. Pasquali and co-workers reported similar effects in the preferential orientation of Au NRs on carbon nanotube bundles.[41] Finally, upon sample

DOI: 10.1021/acsami.7b06273
ACS Appl. Mater. Interfaces 2017, 9, 25513−25521

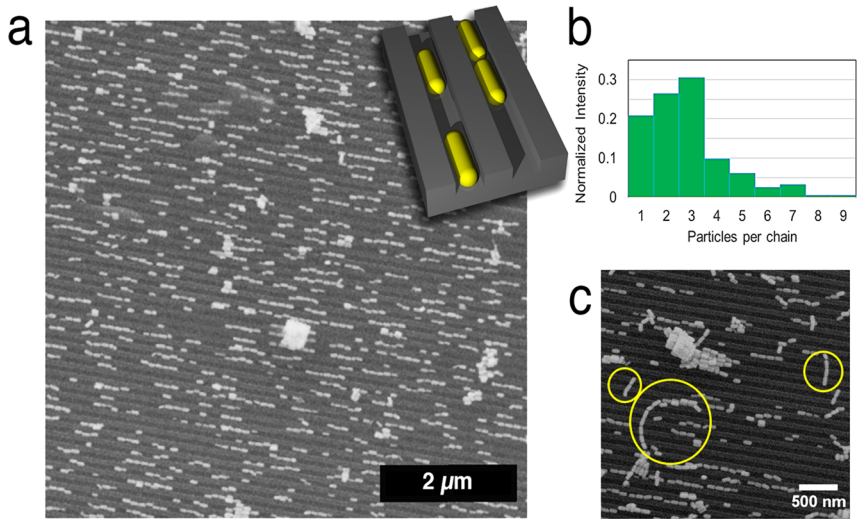

Figure 3. Confinement and orientation of Au NRs with D_{NR} = 58 nm into channels (w = 70 nm). (a) Low-magnification SEM image in an intermediate concentration region demonstrating alignment of Au NRs over several μm. (b) SEM image analysis reveals significantly higher population of longer chains for the thick nanorods with an average of 3.0 ± 1.7 rods/chain and 9−11 rods in the longest chains. (c) When washed from the channels, some nanorods maintain their end-to-end alignment, as shown in the regions highlighted in yellow.

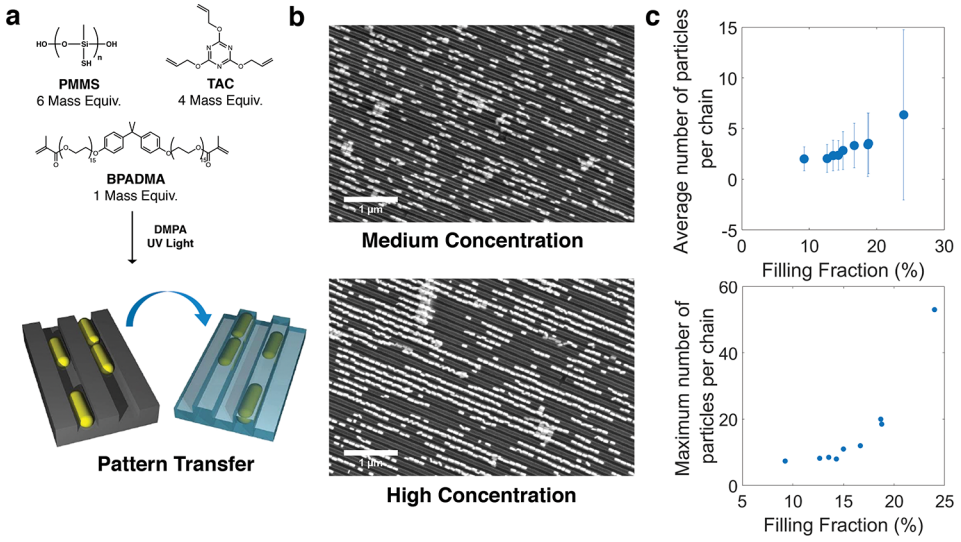

Figure 4. (a) Schematic representation of the PMMS elastomer reaction and pattern-transfer procedure. (b) SEM image of PMMS elastomer films at regions of medium and high nanorod concentration showing high fidelity of the nanorod pattern after transfer from the grating. (c) Image analysis of SEM images showing the average (top) and maximum (bottom) number of Au NRs per chain as a function of the Au NR filling fraction.

drying, the evaporation of the water from the channels generates flow fields that carry the entrained NRs to the air−liquid−substrate interface and deposit them along the channel walls (cf. Figure 1c). The evaporation-mediated hydrodynamic forces in the channels are analogous to those observed in evaporating cylindrical droplets with pinned contact lines. Grogan et al. previously observed *in situ* alignment of Au NRs along contact lines,[42] and Strano et al. demonstrated the efficacy of flow fields within evaporating cylindrical droplets in aligning and positioning the suspended carbon nanotubes on a substrate along the pinning direction.[43] They showed that the normal component of the fluid velocity perpendicular to the pinned edge is directly dependent on the evaporation rate per unit length. If the evaporation rate is faster than the rotational diffusion of the nanorods within the channels, the nanorods may not have sufficient time to reorient within the channels and can be trapped in a tilted configuration relative to the channel walls, as shown in the circled regions of Figure 2a. This is particularly important in the current confinement configuration since it is known that the rotational diffusion of rods near walls can be significantly slower, especially in the presence of electrostatic interactions,[44] emphasizing the importance of the evaporation rate when using gratings to create aligned nanorod assemblies. In fact, effects of slower evaporation were observed near the bottom of the grating (cf. Figure 1a) where the meniscus took longer to dry. In these regions, denser assemblies of nanorods were observed, as shown later, but a two-file configuration was preserved up to a filling factor of ∼25%, beyond which side-by-side NR assemblies start to dominate (Supporting Information, Figure S8).

The case of thin nanorods within channels that are much wider and deeper than the rod thickness is particularly interesting in that the rods not only can occupy different positions along the width of the channels, but also have the

DOI: 10.1021/acsami.7b06273
ACS Appl. Mater. Interfaces 2017, 9, 25513−25521

ability to adhere to the sides of the channels at different vertical locations. Inspired by this, we hypothesized that if the Au NR diameter was commensurate with the channel width, we could achieve significantly better order as rotational diffusion and horizontal positioning of Au NRs within the channel would be restricted. For Au NRs with D_{NR} = 58 nm, the nanorods order in a single file within the groove since the channel can no longer accommodate multiple nanorods. Here too, measurements were performed over regions of low, intermediate, and high nanorod concentrations. Representative SEM images of these regions are shown in the Supporting Information, Figure S9. Figure 3a represents an intermediate nanorod concentration region and shows that the nanorods primarily arrange into end-to-end assemblies over micron-scale areas with approximately 3 nanorods/chain (Figure 3b). In regions that have higher concentrations of Au NRs, superstructures of end-to-end nanorod chains with tens of rods each can be obtained, as shown later. Interestingly, these end-to-end assemblies appear to be stable even after being washed out of the channels. Figure 3c shows several intact chains of Au NRs that remain after the sample was rinsed with water, an hour after it was dried. This process suggests new avenues for harvesting end-to-end nanorod assemblies to use in solutions or in polymeric materials. Moreover, such a close proximity of the nanorods within the chains opens up new possibilities for the design of ultrasmall optical resonators for tunable antennae, filters, and biosensors.[45] While it is not completely clear why the chains retain their integrity after being washed from the channels, we hypothesize that this could result from lower surfactant coverage at the nanorod tips, and strong van der Waals interactions between adjacent particles.

The silicon gratings that template the self-assembly present several obstacles for using the Au NR structures in many applications, primarily because of their lack of optical transparency and high elastic modulus. For a transfer of the Au NRs into a flexible polymeric material that is suitable for optical applications, a solution of triallyl cyanurate (TAC), bisphenol A dimethacrylate (BPADMA), and poly-(methylmercaptosiloxane) (PMMS) was drop-cast on the gold-patterned gratings and UV-photocured for 2 min using 2,2-dimethoxy-2-phenylacetophenone (DMPA) as a radical initiator, as shown in Figure 4a. The low viscosity of the PMMS solution allows the effective wetting of both the grating and rod structures, and the thiol groups ensure strong binding to the nanorods, resulting in an excellent pattern transfer. The cured PMMS elastomer was immediately separated from the silicon grating, resulting in a Au NR/polymer nanocomposite. The SEM images in Figure 4b show the precision of the imprinted grating structure and the effectiveness of the thiol-terminated PMMS in lifting the gold nanorod assemblies without disturbing the long-range order at medium (top) and high (bottom) concentrations. These concentrations correspond to fill factors of approximately 18% and 24%, respectively. Image analysis (Figure 4c) indicates that both the average and maximum number of Au NRs per chain increase as the fill factor increases from approximately 10% to 24%. The average number of Au NRs per chain increases from 2 to 6, while the maximum number per chain increases from 8 to 53. In principle, the same grating can be reused to generate additional polymer imprints, and the mechanical properties of the nanocomposite can be tuned by varying the relative amounts of PMMS, TAC, and BPADMA, as shown previously by Campos and co-workers.[46] When poly(dimethylsiloxane) (SYLGUARD 184, PDMS) was used in place of PMMS, no Au NRs were transferred, highlighting the importance of the PMMS thiol group in the pattern-transfer process. However, the choice of the elastomer is determined by its affinity to the employed nanoparticles, and other suitable elastomers could be used for other nanoparticle compositions.

The optical properties of the Au NR composites were probed using dark field scattering spectroscopy. Measurements of the polymers containing the transferred Au NRs show polarization dependence in the observed dark field scattering intensity. Integrated dark field scattering intensities, from 350 to 1000 nm, for nanocomposites containing the thin (dashed lines) and thick (solid lines) Au NRs are shown in Figure 5, along with the scattering intensity of a patterned PMMS elastomer containing no nanorods (bottom). The signal from the blank PMMS sample shows no angular dependence in the scattering intensity, demonstrating that the anisotropic scattering observed in the nanocomposite samples is not due to the textured substrate. For the nanorod composites, the scattering exhibits a minimum at 90° for light that is polarized perpendicular to the direction of the Au NR alignment, implying that the localized surface plasmon resonance (LSPR) of the nanorod assemblies is not being excited.

The degree of Au NR alignment can be quantified by defining an orientation order parameter $S = (A_{\parallel} - A_{\perp})/(A_{\parallel} + 2A_{\perp})$, where $A_{\parallel}$ and $A_{\perp}$ refer to the scattering intensity measured for polarizer angles which are parallel and perpendicular to the direction of the Au NR alignment, respectively, measured at the LSPR wavelength. For perfectly oriented Au NRs, $S \approx 1$, whereas $S = 0$ for isotropic assemblies. To account for uncertainties in the polarizer angles and quantitatively obtain values for $A_{\parallel}$ and $A_{\perp}$, we fit the dark field scattering intensities to a squared cosine function, and the maximum and minimum values of the function were assigned to $A_{\parallel}$ and $A_{\perp}$, respectively. Under this approach, the calculated order parameter $S \approx 0.04$ for both Au NR composites, which is considerably lower than expected given the large degree of alignment observed in the SEM images shown in Figures 2–4. However, we note that the integration of the scattering intensity over all wavelengths and the position of the LSPR in the assemblies all contribute to an artificially low difference between the scattering intensity at 0° and 90°(for more information see the Supporting Information, Section 4). Though this low difference results in a value of S that is not representative of the true orientational order within the sample, the dark field scattering measurements demonstrate the anisotropic optical properties that the Au NR composites possess. Indeed, 2D orientational analysis of the SEM images reveals remarkable alignment of the nanorods along the channels (see Figure 5b) with average 2D order parameter of $S_{2D} = 0.83 \pm 0.02$ for the thin nanorod sample and $S_{2D} = 0.92 \pm 0.01$ for the thick nanorod sample. This proximity of the order parameter to unity confirms the effectiveness of our procedure in obtaining 1D alignment of nanorods. The S_{2D} values calculated for the two samples are in agreement with the fwhm of the angular dependence of the normalized orientational probabilities (Figure S7), and quantitatively demonstrate the higher degree of alignment obtained in samples with commensurate rod and channel widths.

CONCLUSION

In summary, we have demonstrated a simple, yet scalable, approach for positioning and orienting Au NRs over large

DOI: 10.1021/acsami.7b06273
ACS Appl. Mater. Interfaces 2017, 9, 25513–25521

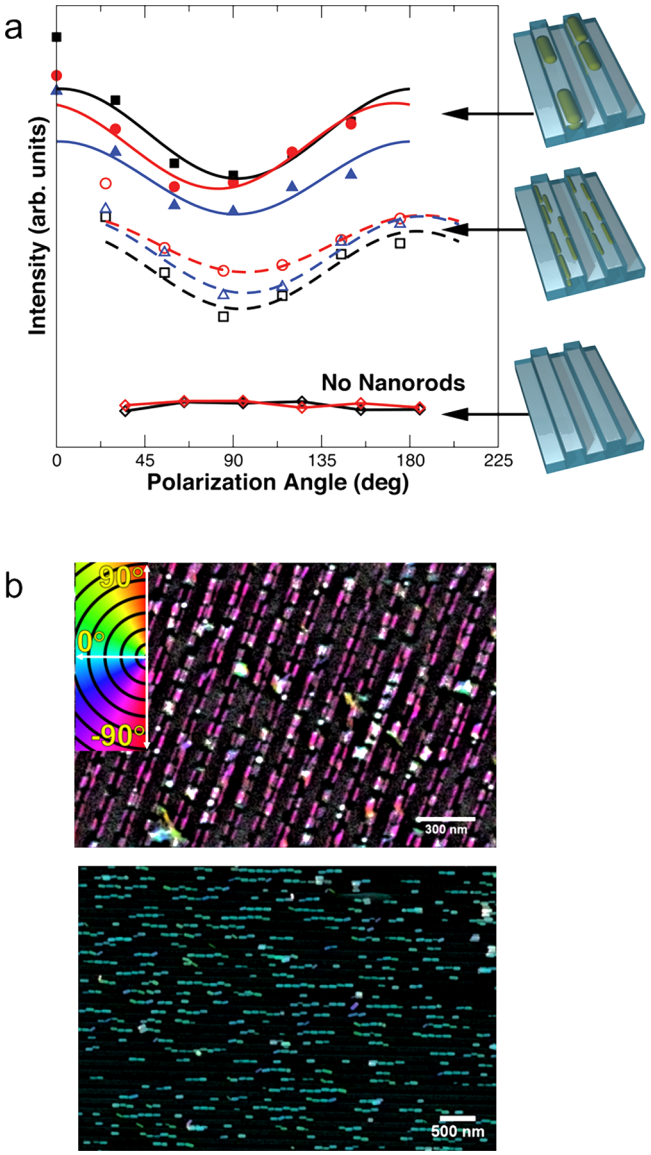

Figure 5. (a) Dark field scattering intensity as a function of polarization angle for elastomers with thick (—, top) and thin (– – –, middle) nanorod samples, and for the pure elastomer (—, bottom). The intensity for both nanorod samples shows a minimum at polarization angles of 90°, demonstrating a large degree of alignment of the nanorods within the elastomers along the channel direction. Colored lines represent measurements from different regions of the sample. (b) Color-coded directionality of thin (top) and thick (bottom) nanorods, showing remarkable alignment of the rods along the channel direction.

length scales using capillary action in drop-cast suspensions on nanostructured linear stamps. Au NRs that are much thinner than the channel width form a unique two-file assembly along the channel walls over a wide concentration range before transitioning into a side-by-side assembly that fills the entire width of the channel, as observed in previous studies. Au NRs with widths that are commensurate with the channel width form single-file assemblies. We hypothesize these configurations are due to strong van der Waals interactions between Au and Si, which may explain why two-file Au NR orientations have not been observed in previous studies. Future experiments which vary both the nanorod material (e.g., Ag or Si), as well as the stamp material, will be important in definitively establishing the mechanism which drives the formation of these assemblies. From an application standpoint, such assemblies have been theoretically shown to amplify plasmon coupling and enhance near-infrared tunability, which are of the utmost importance in the design and fabrication of nanoantennae. We validated the efficacy of transferring the aligned assemblies to a polymer matrix for later use in devices and applications. In the future, we envision applying a selective coating that preferentially adheres to the nanorods (and not to the grating material), where soft coatings can be used for applications requiring flexible Au NR chains and hard coatings for generating rigid chain structures. By the additional employment of dissolvable substrates, the nanorod chains can be retrieved and resuspended, thus offering a myriad of possibilities for easy harvesting and utilization of long Au NR chains. For example, in applications requiring well-defined chain lengths, the resuspended nanorod chains can be length-sorted using ultracentrifugation techniques that have been previously utilized in the fluid-phase sorting of carbon nanotubes.[47,48] While beyond the scope of the present study, these techniques are anticipated to play a vital role in synthesizing high-quality polymer-based optical materials.

■ ASSOCIATED CONTENT

Supporting Information

The Supporting Information is available free of charge on the ACS Publications website at DOI: 10.1021/acsami.7b06273.

Nanostamp cross section, small-angle neutron scattering (SANS) characterization, SEM of PMMS imprint, discussion of dark field scattering spectroscopy results, and orientational analysis of SEM micrographs (PDF)

■ AUTHOR INFORMATION

Corresponding Authors

*E-mail: ashkarra@ornl.gov.
*E-mail: hore@case.edu.

ORCID

Rana Ashkar: 0000-0003-4075-2330
Michael J. A. Hore: 0000-0003-2571-2111
Nicholas J. Greybush: 0000-0001-5784-654X

Present Address

¶Xingchen Ye: Department of Chemistry, Indiana University, Bloomington, IN 47405, United States.

Author Contributions

◆R.A. and M.J.A.H. contributed equally to this work.

Notes

The authors declare no competing financial interest.

■ ACKNOWLEDGMENTS

The identification of commercial products or experimental methods does not imply endorsement by the National Institute of Standards and Technology nor does it imply that these are the best for the purpose. This work utilized neutron scattering facilities supported in part by the National Science Foundation (NSF) under Agreement DMR-0944772. Research at ORNL's Spallation Neutron Source was sponsored by the Scientific User Facilities Division, Office of Basic Energy Sciences, U.S. Department of Energy. C.B.M., C.R.K., and N.J.G. thank NSF/MRSEC (DMR-1120901). R.A. acknowledges the support of ORNL's Neutron Sciences Directorate Clifford G. Shull Fellowship program. R.A. thanks Dr. Christian Long for his help with preliminary AFM measurements. The authors thank

DOI: 10.1021/acsami.7b06273
ACS Appl. Mater. Interfaces 2017, 9, 25513−25521

Prof. Lüis M. Campos (Columbia University) for fruitful discussions regarding PMMS elastomer compositions.

REFERENCES

(1) Jain, P. K.; Eustis, S.; El-Sayed, M. A. Plasmon coupling in nanorod assemblies: Optical Absorption, Discrete Dipole Approximation Simulation, and Exciton-Coupling Model. *J. Phys. Chem. B* **2006**, *110* (37), 18243−18253.

(2) Hore, M. J. A.; Composto, R. J. Functional Polymer Nanocomposites Enhanced by Nanorods. *Macromolecules* **2014**, *47* (3), 875−887.

(3) Kosako, T.; Kadoya, Y.; Hofmann, H. F. Directional Control of Light by a Nano-Optical Yagi-Uda Antenna. *Nat. Photonics* **2010**, *4* (5), 312−315.

(4) Tabor, C.; Van Haute, D.; El-Sayed, M. A. Effect of Orientation on Plasmonic Coupling between Gold Nanorods. *ACS Nano* **2009**, *3* (11), 3670−3678.

(5) Funston, A. M.; Novo, C.; Davis, T. J.; Mulvaney, P. Plasmon Coupling of Gold Nanorods at Short Distances and in Different Geometries. *Nano Lett.* **2009**, *9* (4), 1651−1658.

(6) Park, K.; Koerner, H.; Vaia, R. A. Depletion-Induced Shape and Size Selection of Gold Nanoparticles. *Nano Lett.* **2010**, *10* (4), 1433−1439.

(7) Nepal, D.; Park, K.; Vaia, R. A. High-Yield Assembly of Soluble and Stable Gold Nanorod Pairs for High-Temperature Plasmonics. *Small* **2012**, *8* (7), 1013−1020.

(8) Hore, M. J. A.; Frischknecht, A. L.; Composto, R. J. Nanorod Assemblies in Polymer Films and Their Dispersion-Dependent Optical Properties. *ACS Macro Lett.* **2012**, *1* (1), 115−121.

(9) Frischknecht, A. L.; Hore, M. J. A.; Ford, J.; Composto, R. J. Dispersion of Polymer-Grafted Nanorods in Homopolymer Films: Theory and Experiment. *Macromolecules* **2013**, *46* (7), 2856−2869.

(10) Zhang, S.-Y.; Regulacio, M. D.; Han, M.-Y. Self-Assembly of Colloidal One-Dimensional Nanocrystals. *Chem. Soc. Rev.* **2014**, *43* (7), 2301−2323.

(11) Nie, Z.; Fava, D.; Kumacheva, E.; Zou, S.; Walker, G. C.; Rubinstein, M. Self-Assembly of Metal-Polymer Analogues of Amphiphilic Triblock Copolymers. *Nat. Mater.* **2007**, *6* (8), 609−614.

(12) Nie, Z. H.; Fava, D.; Rubinstein, M.; Kumacheva, E. "Supramolecular" Assembly of Gold Nanorods End-Terminated with Polymer "Pom-Poms": Effect of Pom-Pom Structure on the Association Modes. *J. Am. Chem. Soc.* **2008**, *130* (11), 3683−3689.

(13) Wang, Y.; DePrince, A. E.; Gray, S. K.; Lin, X.-M.; Pelton, M. Solvent-Mediated End-to-End Assembly of Gold Nanorods. *J. Phys. Chem. Lett.* **2010**, *1* (18), 2692−2698.

(14) Caswell, K. K.; Wilson, J. N.; Bunz, U. H. F.; Murphy, C. J. Preferential End-to-End Assembly of Gold Nanorods by Biotin−Streptavidin Connectors. *J. Am. Chem. Soc.* **2003**, *125* (46), 13914−13915.

(15) Zhou, X.; Wang, Y.; Zhong, L.; Bao, S.; Han, Y.; Ren, L.; Zhang, Q. Rational Design of Oriented Assembly of Gold Nanospheres with Nanorods by Biotin-Streptavidin Connectors. *Nanoscale* **2012**, *4* (20), 6256−6259.

(16) Ferrier, R. C.; Lee, H. S.; Hore, M. J. A.; Caporizzo, M.; Eckmann, D. M.; Composto, R. J. Gold Nanorod Linking to Control Plasmonic Properties in Solution and Polymer Nanocomposites. *Langmuir* **2014**, *30* (7), 1906−1914.

(17) Leung, F. C.-M.; Leung, S. Y.-L.; Chung, C. Y.-S.; Yam, V. W.-W. Metal−Metal and $\pi-\pi$ Interactions Directed End-to-End Assembly of Gold Nanorods. *J. Am. Chem. Soc.* **2016**, *138* (9), 2989−2992.

(18) Holzner, F.; Kuemin, C.; Paul, P.; Hedrick, J. L.; Wolf, H.; Spencer, N. D.; Duerig, U.; Knoll, A. W. Directed Placement of Gold Nanorods Using a Removable Template for Guided Assembly. *Nano Lett.* **2011**, *11* (9), 3957−3962.

(19) Lai, F.; Borca-Tasciuc, T.; Plawsky, J. Controlling Directed Self-Assembly of Gold Nanorods in Patterned PS-b-PMMA Thin Films. *Nanotechnology* **2015**, *26* (5), 055301.

(20) Nepal, D.; Onses, M. S.; Park, K.; Jespersen, M.; Thode, C. J.; Nealey, P. F.; Vaia, R. A. Control over Position, Orientation, and Spacing of Arrays of Gold Nanorods Using Chemically Nanopatterned Surfaces and Tailored Particle-Particle-Surface Interactions. *ACS Nano* **2012**, *6* (6), 5693−5701.

(21) Ahmed, W.; Glass, C.; Kooij, E. S.; van Ruitenbeek, J. M. Tuning the Oriented Deposition of Gold Nanorods on Patterned Substrates. *Nanotechnology* **2014**, *25* (3), 035301.

(22) Hamon, C.; Novikov, S.; Scarabelli, L.; Basabe-Desmonts, L.; Liz-Marzan, L. M. Hierarchical Self-Assembly of Gold Nanoparticles into Patterned Plasmonic Nanostructures. *ACS Nano* **2014**, *8* (10), 10694−10703.

(23) Deshmukh, R. D.; Liu, Y.; Composto, R. J. Two-Dimensional Confinement of Nanorods in Block Copolymer Domains. *Nano Lett.* **2007**, *7* (12), 3662−3668.

(24) Murphy, C. J.; Orendorff, C. J. Alignment of Gold Nanorods in Polymer Composites and on Polymer Surfaces. *Adv. Mater.* **2005**, *17* (18), 2173−2177.

(25) Roskov, K. E.; Kozek, K. A.; Wu, W.-C.; Chhetri, R. K.; Oldenburg, A. L.; Spontak, R. J.; Tracy, J. B. Long-Range Alignment of Gold Nanorods in Electrospun Polymer Nano/Microfibers. *Langmuir* **2011**, *27* (23), 13965−13969.

(26) Ahmad, I.; Jansen, H. P.; Zandvliet, H. J. W.; Kooij, E. S. Hydrodynamic Confinement and Capillary Alignment of Gold Nanorods. *Nanotechnology* **2016**, *27* (2), 025301.

(27) Tebbe, M.; Mayer, M.; Glatz, B. A.; Hanske, C.; Probst, P. T.; Muller, M. B.; Karg, M.; Chanana, M.; Konig, T. A. F.; Kuttner, C.; Fery, A. Optically Anisotropic Substrates via Wrinkle-Assisted Convective Assembly of Gold Nanorods on Macroscopic Areas. *Faraday Discuss.* **2015**, *181*, 243−260.

(28) Kuemin, C.; Nowack, L.; Bozano, L.; Spencer, N. D.; Wolf, H. Oriented Assembly of Gold Nanorods on the Single-Particle Level. *Adv. Funct. Mater.* **2012**, *22* (4), 702−708.

(29) Kuemin, C.; Stutz, R.; Spencer, N. D.; Wolf, H. Precise Placement of Gold Nanorods by Capillary Assembly. *Langmuir* **2011**, *27* (10), 6305−6310.

(30) Flauraud, V.; Mastrangeli, M.; Bernasconi, G. D.; Butet, J.; Alexander, D. T. L.; Shahrabi, E.; Martin, O. J. F.; Brugger, J. Nanoscale Topographical Control of Capillary Assembly of Nanoparticles. *Nat. Nanotechnol.* **2016**, *12* (1), 73−80.

(31) Ye, X.; Jin, L.; Caglayan, H.; Chen, J.; Xing, G.; Zheng, C.; Doan-Nguyen, V.; Kang, Y.; Engheta, N.; Kagan, C. R.; Murray, C. B. Improved Size-Tunable Synthesis of Monodisperse Gold Nanorods through the Use of Aromatic Additives. *ACS Nano* **2012**, *6* (3), 2804−2817.

(32) Ye, X.; Zheng, C.; Chen, J.; Gao, Y.; Murray, C. B. Using Binary Surfactant Mixtures To Simultaneously Improve the Dimensional Tunability and Monodispersity in the Seeded Growth of Gold Nanorods. *Nano Lett.* **2013**, *13* (2), 765−771.

(33) Hore, M. J. A.; Composto, R. J. Nanorod Self-Assembly for Tuning Optical Absorption. *ACS Nano* **2010**, *4* (11), 6941−6949.

(34) Gomez-Grana, S.; Hubert, F.; Testard, F.; Guerrero-Martinez, A.; Grillo, I.; Liz-Marzan, L. M.; Spalla, O. Surfactant (Bi)Layers on Gold Nanorods. *Langmuir* **2012**, *28* (2), 1453−1459.

(35) Hore, M. J. A.; Ye, X.; Ford, J.; Gao, Y.; Fei, J.; Wu, Q.; Rowan, S. J.; Composto, R. J.; Murray, C. B.; Hammouda, B. Probing the Structure, Composition, and Spatial Distribution of Ligands on Gold Nanorods. *Nano Lett.* **2015**, *15* (9), 5730−5738.

(36) Deegan, R. D.; Bakajin, O.; Dupont, T. F.; Huber, G.; Nagel, S. R.; Witten, T. A. Capillary Flow as the Cause of Ring Stains from Dried Liquid Drops. *Nature* **1997**, *389* (6653), 827−829.

(37) Yunker, P. J.; Still, T.; Lohr, M. A.; Yodh, A. G. Suppression of the Coffee-Ring Effect by Shape-Dependent Capillary Interactions. *Nature* **2011**, *476* (7360), 308−311.

(38) Sharma, Y.; Dhawan, A. Hybrid Nanoparticle−Nanoline Plasmonic Cavities as SERS Substrates with Gap-Controlled Enhancements and Resonances. *Nanotechnology* **2014**, *25* (8), 085202.

(39) Liddle, J. A.; Cui, Y.; Alivisatos, P. Lithographically Directed Self-Assembly of Nanostructures. *J. Vac. Sci. Technol., B: Microelectron. Process. Phenom.* **2004**, *22* (6), 3409−3414.

DOI: 10.1021/acsami.7b06273
ACS Appl. Mater. Interfaces 2017, 9, 25513−25521

(40) Onsager, L. The Effects of Shape on the Interaction of Colloidal Particles. *Ann. N. Y. Acad. Sci.* **1949**, *51* (4), 627−659.
(41) Dan, B.; Wingfield, T. B.; Evans, J. S.; Mirri, F.; Pint, C. L.; Pasquali, M.; Smalyukh, I. I. Templating of Self-Alignment Patterns of Anisotropic Gold Nanoparticles on Ordered SWNT Macrostructures. *ACS Appl. Mater. Interfaces* **2011**, *3* (9), 3718−3724.
(42) Grogan, J. M.; Schneider, N. M.; Ross, F. M.; Bau, H. H. The Nanoaquarium: A New Paradigm in Electron Microscopy. *J. Indian Inst. Sci.* **2012**, *92* (2), 295−308.
(43) Sharma, R.; Lee, C. Y.; Choi, J. H.; Chen, K.; Strano, M. S. Nanometer Positioning, Parallel Alignment, and Placement of Single Anisotropic Nanoparticles Using Hydrodynamic Forces in Cylindrical Droplets. *Nano Lett.* **2007**, *7* (9), 2693−2700.
(44) Haghighi, M.; Tahir, M. N.; Tremel, W.; Butt, H.-J.; Steffen, W. Translational and Rotational Diffusion of Gold Nanorods Near a Wall. *J. Chem. Phys.* **2013**, *139* (6), 064710.
(45) Li, Z.; Butun, S.; Aydin, K. Touching Gold Nanoparticle Chain Based Plasmonic Antenna Arrays and Optical Metamaterials. *ACS Photonics* **2014**, *1* (3), 228−234.
(46) Campos, L. M.; Truong, T. T.; Shim, D. E.; Dimitriou, M. D.; Shir, D.; Meinel, I.; Gerbec, J. A.; Hahn, H. T.; Rogers, J. A.; Hawker, C. J. Applications of Photocurable PMMS Thiol−Ene Stamps in Soft Lithography. *Chem. Mater.* **2009**, *21* (21), 5319−5326.
(47) Arnold, M. S.; Green, A. A.; Hulvat, J. F.; Stupp, S. I.; Hersam, M. C. Sorting Carbon Nanotubes by Electronic Structure Using Density Differentiation. *Nat. Nanotechnol.* **2006**, *1* (1), 60−65.
(48) Fagan, J. A.; Becker, M. L.; Chun, J.; Hobbie, E. K. Length Fractionation of Carbon Nanotubes Using Centrifugation. *Adv. Mater.* **2008**, *20* (9), 1609−1613.

DOI: 10.1021/acsami.7b06273
ACS Appl. Mater. Interfaces 2017, 9, 25513−25521